

## **Influence of Chain Length of Gradient and Block Copoly(2-oxazoline)s on Self-Assembly and Drug Encapsulation**

Ondrej Sedlacek,<sup>a,b</sup> Valentin Bardoula,<sup>a,c</sup> Elina Vuorimaa-Laukkanen,<sup>d</sup> Lars Gedda,<sup>e</sup> Katarina Edwards,<sup>e</sup> Aurel Radulescu,<sup>f</sup> Grigoriy A. Mun,<sup>g</sup> Yong Guo,<sup>h,i</sup> Junnian Zhou,<sup>i,j</sup> Hongbo Zhang,<sup>i</sup> Véronique Nardello-Rataj,<sup>c</sup> Sergey Filippov,<sup>g,i</sup> Richard Hoogenboom<sup>a,\*</sup>

<sup>a</sup>Supramolecular Chemistry Group, Department of Organic and Macromolecular Chemistry, Ghent University, Krijgslaan 281 S4, B-9000 Ghent, Belgium.

<sup>b</sup>Department of Physical and Macromolecular Chemistry, Faculty of Science, Charles University, Hlavova, 2030, 128 40 Prague 2, Czech Republic

<sup>c</sup>Centrale Lille, Université de Lille, CNRS, Université Artois, UMR 8181-UCCS-Unité de Catalyse et Chimie du Solide, Lille, France

<sup>d</sup>Tampere University of Technology, Tampere, Finland

<sup>f</sup>Department of Chemistry –Ångström Laboratory, Uppsala University, Sweden

<sup>f</sup>Jülich Centre for Neutron Science (JCNS) at Heinz Maier-Leibnitz Zentrum (MLZ) Forschungszentrum Jülich GmbH Lichtenbergstr. 1, 85748 Garching, Germany.

<sup>g</sup>Department of Chemistry & Technology of Organic Materials, Polymers and Natural Compounds, al Faraby Kazakh National University, 71, al-Faraby av., 050040, Almaty, Republic of Kazakhstan

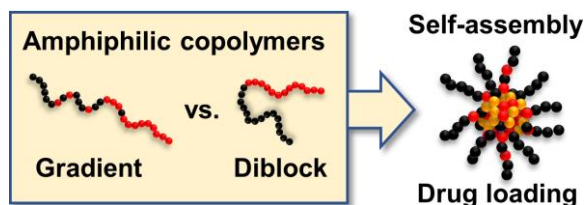
<sup>h</sup>Department of Endocrinology, Key Laboratory of National Health & Family Planning Commission for Male Reproductive Health, National Research Institute for Family Planning, Beijing 100081, China.

<sup>i</sup>Pharmaceutical Sciences Laboratory and Turku Bioscience Center, of Åbo Akademi University and Turku Bioscience, Turku 20520, Finland.

<sup>j</sup>Experimental Hematology and Biochemistry Lab, Beijing Institute of Radiation Medicine, Beijing 100850, China;

E-mail: [richard.hoogenboom@ugent.be](mailto:richard.hoogenboom@ugent.be)

## TOC graphic:



## Abstract

Amphiphilic gradient copolymers represent a promising alternative to extensively used block copolymers due to their facile one-step synthesis by statistical copolymerization of monomers of different reactivity. Herein, an in-depth analysis is provided of micelles based on amphiphilic gradient poly(2-oxazoline)s with different chain lengths to evaluate their potential for micellar drug delivery systems and compare them to the analogous diblock copolymer micelles. Size, morphology, and stability of self-assembled nanoparticles, loading of hydrophobic drug curcumin, as well as cytotoxicities of the prepared nanoformulations are examined using copoly(2-oxazoline)s with varying chain lengths and comonomer ratios. In addition to several interesting differences between the two copolymer architecture classes, such as more compact self-assembled structures with faster exchange dynamics for the gradient copolymers, it is concluded that gradient copolymers provide stable curcumin nanoformulations with comparable drug loadings to block copolymer systems and benefit from more straightforward copolymer synthesis. The study demonstrates the potential of amphiphilic gradient copolymers as a versatile platform for the synthesis of new polymer therapeutics.

## 1. Introduction

In the past decades, polymeric nonionic surfactants emerged as essential materials for preparing diverse disperse systems with a broad range of applications.[1-4] Generally, they are represented by amphiphilic copolymers containing both hydrophilic and hydrophobic segments in the same chain.[5, 6] This amphiphilicity usually leads to their self-assembly in an aqueous environment into nanoparticles of various morphologies, such as micelles, cylindrical micelles, and vesicles, with the first containing hydrophobic core stabilized by a hydrophilic shell. Micelles based on amphiphilic copolymers generally have higher colloidal stability than micelles based on low molar mass surfactants (e.g., sodium dodecyl sulfate).[7] Among the different amphiphilic copolymer architectures that can be used for the preparation of micelles, block copolymers are most commonly used due to their relatively easy synthesis, using a two-step sequential monomer addition procedure or the use of a preformed polymer as initiator. In the biomedical sciences, amphiphilic block copolymers are particularly useful for the solubilization of poorly water-soluble drugs, improving their maximal dosage and increasing their blood circulation times.[8] As an example, a nanoformulation of the anti-cancer drug paclitaxel encapsulated by poly(ethylene oxide)-block-poly(lactide) (PEO-PLA) copolymer micelles has been clinically approved for the treatment of metastatic breast cancer and advanced lung cancer in South Korea, distributed under the name GenexolPM by Samyang Biopharm.[9]

Amphiphilic gradient copolymers represent an attractive alternative to block copolymers due to their even easier synthesis and tunable properties.[10-12] While the synthesis of block copolymers is essentially a multistep process, gradient copolymers can be synthesized in a single step by statistical copolymerization of monomers with different reactivities, leading to a compositional drift in the formed copolymer.[13] The more reactive monomer is preferentially incorporated into the polymer chain at the beginning of the copolymerization process, while the less reactive one is preferentially incorporated at the end of copolymerization when the first monomer is being depleted. In the case of comonomers with substantially different reactivities, a copolymer with steep gradient architecture (quasi-block) is formed. Such behavior was observed in, e.g., radical copolymerization of (meth)acrylates and (meth)acrylamides with less reactive vinyl esters[14] or cyclic ketene acetals,[15] anionic copolymerizations of functional epoxides,[16] aziridines,[17] styrene/isoprene pair[18] as well as the cationic ring-opening copolymerization (CROP) of different 2-alkyl-2-oxazolines[19-21] and 2-alkyl-2-oxazines.[22] Apart from the difference in monomer reactivities, the monomer distribution

along the polymer chain can be controlled to a certain level by selecting the copolymerization temperature or solvent.[23] Finally, an important advantage of these spontaneously formed amphiphilic gradient copolymers over their block copolymer analogs is the possibility of fine-tuning the self-assembly properties by changing the steepness of the formed gradient, as reported recently.[24]

Poly(2-alkyl-2-oxazoline)s (PAOx) are emerging polymers with rising potential in biomedical sciences.[25-27] Generally, they are synthesized by living cationic ring-opening polymerization (CROP) of 2-alkyl-2-oxazoline monomers leading to well-defined polymers with low molar mass dispersities.[28] The physical properties of PAOx mainly depend on the character of the side-chain substituent.[29] PAOx with short side-chain groups, i.e., poly(2-methyl-2-oxazoline) (PMeOx) and poly(2-ethyl-2-oxazoline) (PEtOx), are water-soluble biocompatible polymers that are particularly suitable for biomedical applications such as drug delivery systems or anti-fouling coatings.[30-32] On the other hand, PAOx with either aromatic or long aliphatic side-chains, e.g., poly(2-phenyl-2-oxazoline) (PPhOx) or poly(2-butyl-2-oxazoline) (PBuOx), are hydrophobic and found their application as core-forming blocks in amphiphilic copolymer nanoformulations.[33]

Several PAOx-based micellar drug delivery systems have been reported.[34, 35] Probably the most promising systems comprise PMeOx–PBuOx–PMeOx triblock copolymers, which allow encapsulation of an extremely high quantity (often >50 wt%) of hydrophobic drugs such as paclitaxel or curcumin.[33] These formulations show excellent anticancer properties both in vitro and in vivo.[36, 37] The main advantages of these systems are the simplicity of preparation and high drug loadings. The cost of the high drug loading is, however, the rapid diffusion-driven “burst release” of the drug from the micelle, which might lead to the premature loss of part of the cytostatic cargo before reaching the target tissue, which represents one of the major drawbacks of such systems. In our study, we use the PPhOx as a core-forming block due to its relative rigidity (glass transition temperature  $T_g = 103\text{--}107\text{ }^\circ\text{C}$ ), as we assume that the rigid “glassy” core could prevent the premature drug leakage compared to the flexible “liquid” core of PBuOx.[29] Furthermore, the PPhOx-based micelles are expected to have higher stability, which can lead to their extended blood plasma circulation times.

Amphiphilic gradient PAOx can be synthesized in a single step by statistical copolymerization of more reactive 2-alkyl-2-oxazolines with less reactive 2-aryl-2-oxazolines.[29] As an example, different reactivities of MeOx and PhOx lead to the formation of an amphiphilic gradient PMeOx-grad-PPhOx copolymer that self-assembles in water into spherical or ellipsoid micelles.[19] The internal structure of these nanoparticles and their block analogs were thoroughly studied by various advanced scattering techniques, including small-angle X-ray scattering (SAXS)/ small-angle neutron scattering (SANS) and light scattering. While the block copolymers assemble into micelles with uniform core density, the gradient copolymers form micelles with the outer part of the core denser than the center due to the chain back-folding, resulting in a smaller diameter of the gradient micelles compared to the block ones.[38] However, we anticipate that this behavior is chain-length dependent and a certain degree of polymerization (DP) is required to enable effective back-folding. Therefore, in this study, we introduce the use of polymer DP as an important parameter for the copolymer self-assembly and drug encapsulation, rather than a variation of the hydrophilic/hydrophobic unit ratio. Despite their indisputable potential, reports on the drug delivery systems based on amphiphilic gradient copolymers are still very sparse. Kronek and co-workers reported the encapsulation of the hydrophobic drug curcumin in amphiphilic gradient PEtOx-grad-poly(2-(4-dodecyloxyphenyl)-2-oxazoline) copolymer micelles.[39] The nanoformulations revealed decent drug-loading (12–22 wt%), excellent in vitro stability and low toxicity. Very recently, Hrubý et al. compared amphiphilic gradient and diblock copolymers of methyl-2-oxazoline (MeOx) with three different aromatic 2-oxazolines, having the total DP of 100.[40] At some comonomer ratios, the gradient copolymer-based nanoformulations showed higher drug loadings than diblock analogs, which was hypothesized to result from a less dense micellar core structure. Despite the recent progress on the self-assembly and drug encapsulation by gradient copoly(2-oxazoline)s, all reported studies were limited to rather short polymers with a maximum DP of 100. As such, there is a lack of knowledge on the effect of the DP of gradient copolymers on their self-assembly and drug encapsulation behavior, which will be addressed for the first time in this work.

This study provides a detailed comparison of the micelles formed by the self-assembly of amphiphilic gradient and diblock copolymers, with systematical variation in their chain length, to assess their potential as drug-delivery vehicles. Therefore, we synthesized a series of amphiphilic PMeOx–PPhOx copolymers having the same hydrophilic/hydrophobic unit ratio

while differing in the polymer architecture (gradient vs. diblock) and the total DP. The self-assembly properties and the micelle dynamics were studied by several light-scattering techniques and Forster resonance energy transfer (FRET) spectroscopy to evaluate the effect of DP and monomer distribution on the self-assembly. Furthermore, different techniques were used for the encapsulation of the hydrophobic drug curcumin and the properties of the formed nanoformulations were critically compared and discussed in order to find an optimal architecture for micellar drug delivery systems.

## **2. Results and discussion**

### **2.1. Copolymer Synthesis**

Amphiphilic gradient PMeOx-grad-PPhOx copolymers were synthesized in a one-step procedure using a microwave-assisted statistical CROP of MeOx and PhOx initiated by methyl p-toluenesulfonate in acetonitrile (Figure 1). Copolymers of two molar contents of MeOx ( $F_{\text{MeOx}} = 0.6$  or  $0.7$  corresponding to 46 wt% MeOx and 57 wt% MeOx, respectively) were prepared in different total chain lengths (DP 30, 40, 60, 80, 100, 120, 150), labeled as G601-7 ( $F_{\text{MeOx}} = 0.6$ ) and G1-7 ( $F_{\text{MeOx}} = 0.7$ ). It was noted that the gradient copolymers with lower MeOx content (G601-7) showed reduced water-solubility, especially at higher total DPs. Therefore, the copolymers with higher MeOx content (G1-7) were used further for the direct comparison of block and gradient copolymers and a series of analogous block copolymers (B1-7) with the same MeOx content ( $F_{\text{MeOx}} = 0.7$ ) was synthesized in two steps by sequential polymerization of MeOx and PhOx. All copolymers were analyzed by  $^1\text{H}$  NMR spectroscopy, revealing the expected molecular composition. Size-exclusion chromatography revealed the formation of relatively well-defined copolymers with a narrow molar mass distribution ( $\mathcal{D} < 1.25$ , Figure S1, Supporting Information). The size-exclusion chromatograms of the gradient and block copolymers with the same DP showed very good agreement, setting a solid ground for the comparison of their self-assembly behavior.

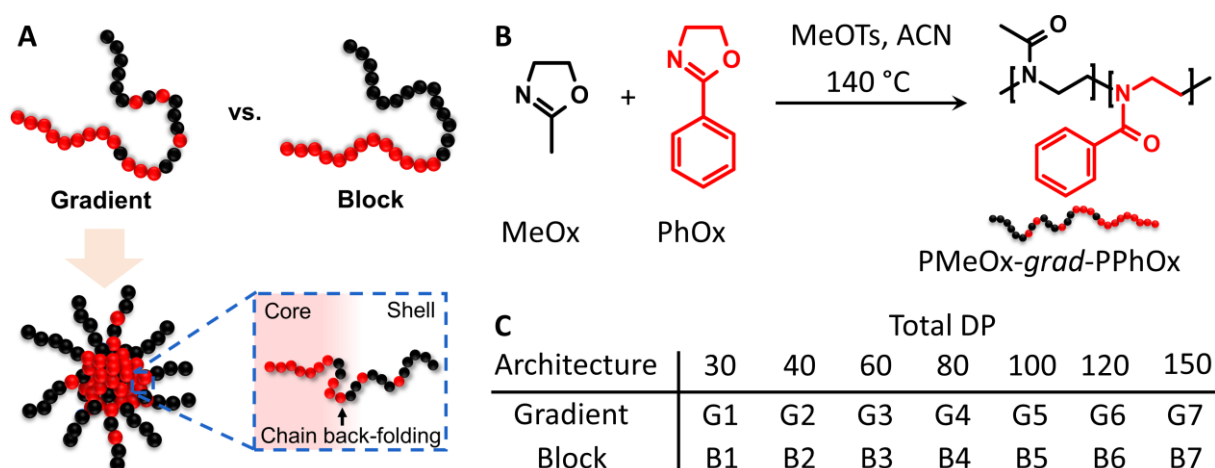


**Figure 1.** Comparison of amphiphilic gradient and diblock copoly(2-oxazoline)s: A) Schematic illustration of both architectures. B) Synthesis of PMeOx-grad-PPhOx copolymers. C) Overview of the synthesized gradient (G1-G7), respectively diblock (B1-7) copolymers having the same MeOx:PhOx ratio of 70:30.

## 2.2. Effect of Copolymer Architecture on Self-Assembly Properties

All synthesized copolymers with  $F_{\text{MeOx}} = 0.7$  were water-dispersible and assembled into nanoparticles upon simple dissolution in water. The size of the nanoparticles was studied by dynamic light scattering (DLS, Figure 2A,B), revealing a significant effect of the total DP on the self-assembly behavior of the block and gradient copolymers. Shorter block and gradient copolymers with a DP below 60 resulted in micelles of nearly the same size. The formation of the large aggregates at the lowest DP 30 can be ascribed to the composition heterogeneity within the individual copolymer chains of these short polymers with on average only 9 hydrophobic PhOx units. On the other hand, the micelles formed by the longer copolymers with a DP above 80 were found to be significantly smaller for the gradient copolymers compared to the block copolymers, which is in agreement with our previous study on the comparison of block and gradient copolymers with DP 100.[19] From these results, it can be hypothesized that a minimal DP of 60–80 (i.e., 18–24 hydrophobic repeating units per chain) is required for efficient back-folding of the gradient copolymer chains, which leads to smaller nanoparticles. The size and morphology of the self-assembled structures were studied by cryogenic transmission electron microscopy (CryoTEM, Figure 2C; Figure S3, Supporting Information), corroborating the DLS data. The size of the nanoparticles increased with the total chain length. Gradient copolymer micelles showed a pure spherical morphology in the whole range of DPs. On the other hand,

analogous block copolymer micelles showed a transition from spherical morphology at lower DPs to a mixture of spherical and worm-like morphology at higher DPs. This contributes to their bigger average size and broader dispersity, as observed by DLS, at higher DP than the gradient copolymer analogs since worm-like aggregates should have higher hydrodynamical diameter bringing additional polydispersity to size distribution. This transition from spherical to worm-like micelles can be ascribed to the increased interfacial tension from the longer hydrophobic blocks. For the gradient copolymer micelles, the absence of this morphological transition may be attributed to a denser core–shell transition region that protects these micelles from fusion in diluted solutions.

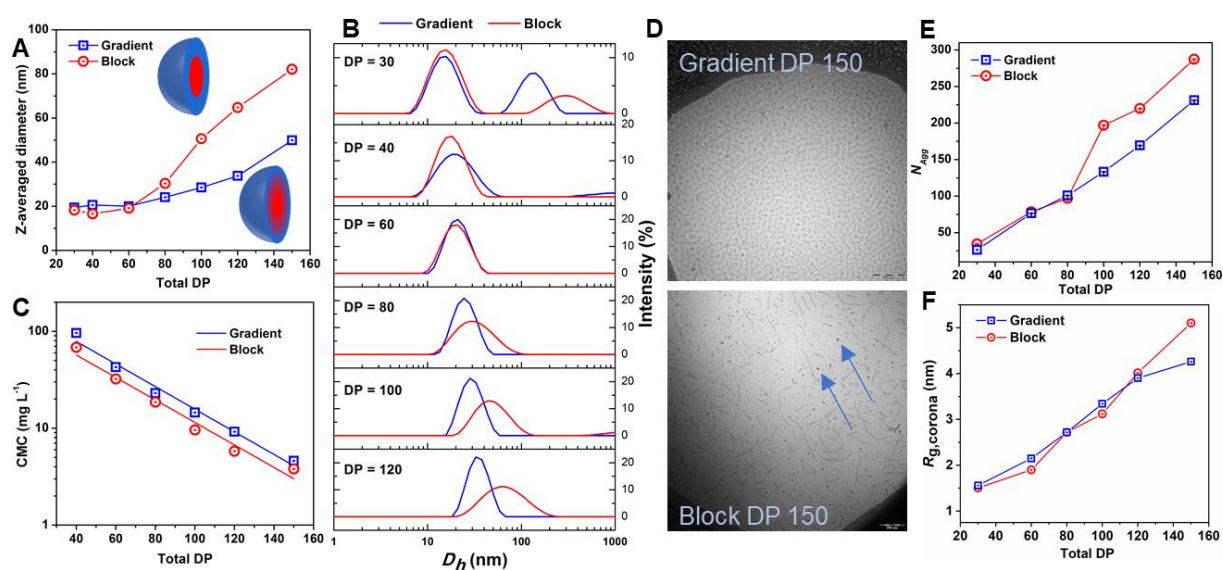


**Figure 2.** Comparison of self-assembly properties of PMeOx–PPhOx amphiphilic gradient and diblock copolymers ( $F_{MeOx} = 0.7$ ) in water. A) Hydrodynamic diameters and B) size distributions of copolymers in water ( $c_{pol} = 10 \text{ mg mL}^{-1}$ ). C) Critical micelle concentrations (CMC) of the synthesized copolymers in PBS. D) CryoTEM images of G7 (top) and B7 (bottom) copolymers in water. Arrows indicate ice crystals artifacts. Scale bars represent 200 nm. E) Aggregation number of copolymers in water as a function of DP. F) The gyration radius of a polymer chain in the nanoparticle corona as a function of polymerization degree (DP) of the copolymer micelles in water.

The structural characteristics of the B and G series of PMeOx–PPhOx micelles were also examined by small-angle neutron scattering (SANS; Figure 2F; Figure S4, Supporting Information). The data were fitted using the block copolymer elliptical micelle model, which

includes four structural parameters extracted from the model fitting to the data ( $N_{agg}$ ,  $\sigma$ ,  $R_g$ , and  $\epsilon$ ). From these fitting parameters, the micellar core radius ( $R_{core}$ ) was calculated (Figure 2F). The low- $q$  region in the SANS data is most highly influenced by variations in the aggregation number ( $N_{agg}$ ).  $N_{agg}$  was extracted from the model and is shown in Figure 2E. We note that the gradient structure and molecular weight of the copolymers significantly impact the structural parameters of the micelles, as will be discussed in the following.

The block copolymer micelle series showed a steeper increase in  $N_{agg}$  with increasing copolymer length compared to the gradient copolymer micelles series  $N_{agg}$  (Table S4, Supporting Information), which is consistent with the trends observed by DLS and CryoTEM. It has previously been reported that  $N_{agg}$  increases as the interfacial tension of the core–corona interface increases.[41] When the interfacial tension is high, the total interfacial area of the micelle system is decreased by increasing  $N_{agg}$ , which also decreases the total number of micelles. In our system, varying the molecular weight and copolymer architecture tunes the core/corona interfacial tensions. D2O is a good solvent for PMeOx and a poor solvent for PPhOx; thus, as the hydrophobic block length increases, the interfacial tension and, respectively,  $N_{agg}$  increases. The behavior observed in both block and gradient copolymer micelle series, in which  $N_{agg}$  increased with increasing the length of the PPhOx block, is consistent with prior studies.[16] However, the gradient copolymer micelles exhibited a less pronounced increase of  $N_{agg}$  as the copolymer molecular weight increased. We consider this as proof that the gradient structure impacts the core–corona interfacial tension due to the existence of additional interphase layers and loop formation.

The SANS experiments showed that spherical micelles are formed at low DP values below 60, whereas ellipsoidal micelles with eccentricity 1.1–2 are formed for copolymers with a DP above 80. This observation is not surprising since the asymmetry of PMeOx–PPhOx micelles was already reported previously.[16] The micellar asymmetry was explained by  $\pi$ – $\pi$  stacking interactions of the phenyl rings in the PhOx block. Another interesting finding is the smaller  $R_g$  value for hydrophilic corona in the gradient copolymer micelles series compared to the micelles of block copolymers with similar molecular weight and composition (Table S4, Supporting Information). Such behavior can be explained by the loops formed in the PMeOx gradient copolymer micelles, resulting from hydrophobic PPhOx patches in between hydrophilic

PMeOx parts. These loops will have a lower  $R_g$  value in comparison with stretched polymer chains of the same length. Furthermore, the loops consist of a lower number of MeOx units, further reducing the  $R_g$  value.

### 2.3. Effect of Copolymer Architecture on Nanoparticle Stability

The stability of the micelles plays a key role in the pharmacokinetic profile of the potential drug-loaded nanoformulations as more stable micelles will have longer blood circulation times. On the other hand, micelles with extremely rigid, vitrified cores show limited excretion and very slow drug release. In solution, self-assembled micelles theoretically exist in equilibrium with their unimers, if no kinetically trapped structures are formed. Upon dilution below their critical micelle concentration (CMC), such equilibrium micelles disassemble into unimers. Herein, the CMC of the prepared PMeOx–PPhOx copolymers was determined to assess the impact of the copolymer architecture and chain length on the equilibrium stability. The obtained CMC values ranged from 3.8 to 96 mg L<sup>-1</sup>, which is in good agreement with previously reported data.[19] Increasing the total length of the copolymers led to increased micelle stability, as indicated by lower CMC values (Figure 2C; Tables S2 and S3, Supporting Information), in line with previous reports.[43] This can be attributed to the larger interfacial tension of the micelles assembled from copolymers with longer hydrophobic segments. The block copolymer micelles are slightly more stable than the gradient analogs, as indicated by slightly lower CMC values, which can be ascribed to the destabilization of the latter by the presence of a small fraction of hydrophilic units in the hydrophobic core.

The micelle-unimer exchange dynamics were studied by time-resolved Förster resonance energy transfer (FRET) of fluorescently labeled micelles (Figure 3; Figure S5 and Table S5, Supporting Information). Two different micelle solutions of the same copolymers containing a minor fraction of covalently labeled copolymers functionalized with either a FRET donor (fluorescein) or a FRET acceptor (rhodamine B) were mixed and the fluorescence intensity of the acceptor (575 nm) was donor (455 nm). Directly after mixing, there is no FRET emission, but when the labeled unimers start to exchange between the micelles, the FRET emission increases due to the colocalization of the FRET donors and FRET acceptors within the same micelles. The increase in FRET emission in time was used to compare the dynamic stability of micelles prepared from gradient copolymer G5 and diblock copolymer B5. This fluorescence increase of the selected FRET dye-couple is rather small; however, it is sufficient for the

purpose of our experiment. The gradient copolymer micelles show a faster increase in FRET emission than the diblock copolymer analogs, presumably due to their higher CMC and, therefore, a higher concentration of unimers leading to faster unimer exchange between micelles. Alternatively, this observation could be explained in terms of the polymer residence time within the micelles, which, like the CMC, is governed by the free energy cost of dissolving the polymeric unimers in the aqueous phase. The measured increase in FRET intensity was fitted with a double exponential plot, revealing two distinct exchange rate constants for each system. This is likely related to the different relative hydrophilicity of the fluorescent labels. The acceptor molecule (rhodamine B) is more hydrophilic than the donor (fluorescein), which lowers the energetic barrier for the micelle-unimer equilibrium for the rhodamine B-labeled copolymers. These rhodamine-labeled unimers are then exchanged at a higher rate (with an exchange half-life ( $t_{1/2}$ ) of 11 min for G5 and 16 min for B5) than the fluorescein-labeled copolymers ( $t_{1/2}$  = 146 min for G5, 218 min for B5). Based on these dynamic exchange experiments, it can be concluded that both G5 and B5 with DP 100 show dynamic unimer exchange and that the diblock copolymer micelles manifest higher stability than the gradient analogs. Besides the micelle-unimer stability, other parameters might influence the stability of micelles in a biological environment, such as their interactions with serum proteins, which leads to their accelerated clearance of the micelles by the mononuclear phagocyte system. As these interactions depend mainly on the structure of the micelle shell, one might expect a difference between both copolymer architectures. However, this biological evaluation is beyond the scope of this article, focusing mainly on synthesis and physicochemical comparison of gradient and block copolymer nanoformulations.

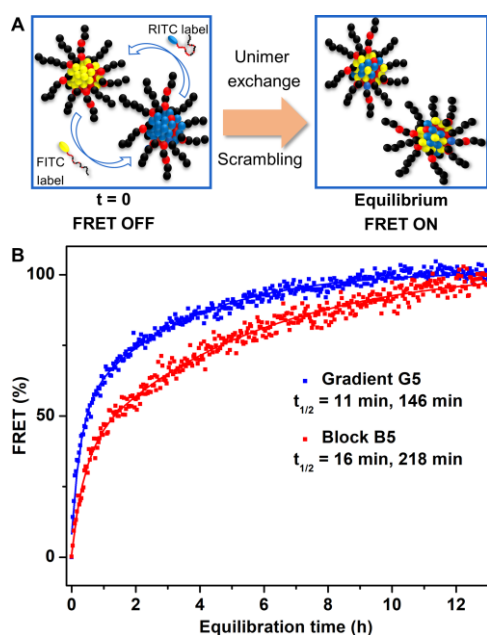


**Figure 3.** Dynamics of unimer exchange between fluorescently labeled micelles determined by the increase of the Förster resonance energy transfer (FRET) after mixing at 25 °C ( $c_{\text{pol}} = 1 \text{ mg mL}^{-1}$ ). (A) Schematic illustration. (B) Comparison of the unimer exchange dynamics of G5 and B5.

#### 2.4. Effect of Copolymer Architecture on Hydrophobic Drug Loading

The drug solubilization ability of the prepared amphiphilic copolymers was investigated using curcumin as a model drug. In contrast to the study of Hrubý and co-workers,[40] who loaded the micelles with relatively hydrophilic drug rifampicin (solubility in PBS reported as  $9.9 \text{ mg mL}^{-1}$ ),[44] curcumin shows negligible solubility in water ( $<8 \text{ } \mu\text{g mL}^{-1}$ ),[45] and, therefore, represents an ideal model compound for our thorough encapsulation study that aims to enhance the solubility of hydrophobic drugs. Inspired by the ultra-high drug loading of poly(2-oxazoline) and poly(2-oxazine)s based micelles as reported by Kabanov and Luxenhofer, we first explored the thin-film rehydration approach (Figure 4A).[33,35,46,47] Therefore, a solution of copolymer (G1-G7 or B1-G7) and curcumin in ethanol was evaporated in a stream of air, forming a thin film in the vial. This film was then re-hydrated in PBS, which led to the formation of drug-loaded nanoparticles. As the solubility of curcumin in water is extremely low, the non-encapsulated or aggregated curcumin was removed by centrifugation. The amount of solubilized curcumin was measured by UV-vis spectroscopy in ethanol (Figure 4B; Table S6, Supporting Information). The final copolymer concentration was kept constant ( $10 \text{ mg mL}^{-1}$ ) while the curcumin feed was varied in the range from 1 to  $4 \text{ mg mL}^{-1}$ . The maximal

drug loading (DL, the weight content of curcumin in the nanoformulation) that could be achieved was 16 wt%. At low copolymer DPs and low curcumin feed, the loading efficiency (LE) was high and the amount of solubilized curcumin increased with curcumin feed. However, the highest curcumin feed (4 mg mL<sup>-1</sup>) led to the formation of a water-insoluble polymer/curcumin precipitate due to the drug-polymer interactions and hydrophobization of the entire system. This effect was more pronounced for copolymers of higher DPs as well as for gradient copolymers compared to block copolymer analogs. Such behavior can be explained by the presence of a small quantity of hydrophobic PPhOx units in the hydrophilic PMeOx segments, which, in solid thin film blend, leads to increased interchain interactions, preventing efficient stabilization of the formed nanoparticles by the hydrophilic corona. As the thin film method was not very efficient for the preparation of curcumin-loaded gradient copolymer nanoformulations, other methods were explored that avoided the formation of a solid blend of curcumin with the copolymer.

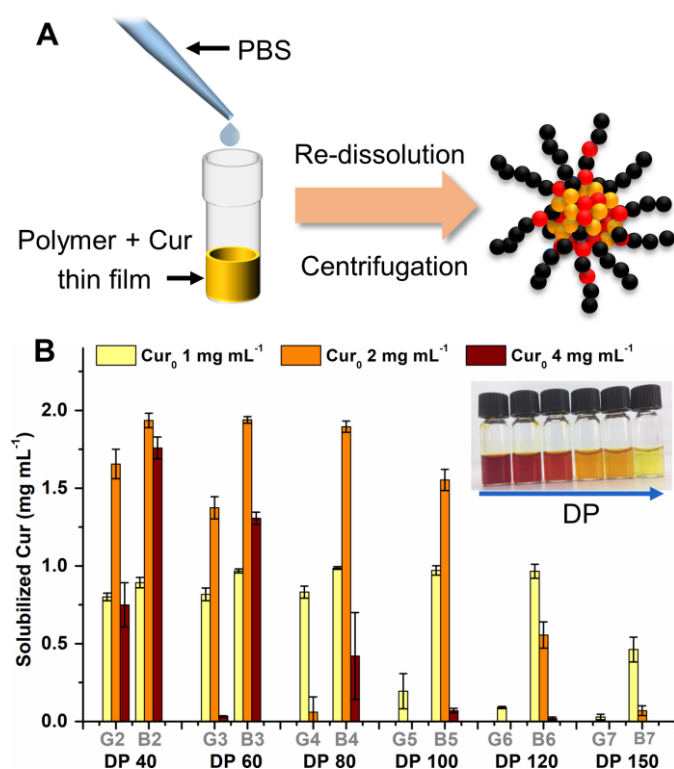


**Figure 4.** Solubilization of curcumin by PMeOx-PPhOx ( $F_{MeOx} = 0.7$ ) gradient (G2-G7) or diblock (B2-B7) copolymers using the thin-film hydration method. A) Schematic illustration of the rehydration method for the preparation of the curcumin-loaded micelles. B) Amount of

curcumin solubilized by amphiphilic copolymers ( $c_{pol} = 10 \text{ mg mL}^{-1}$ ) with the different feed of curcumin, expressed as mean  $\pm$  SD ( $n = 3$ ).

Stable nanoformulations of curcumin-loaded amphiphilic copolymer micelles were obtained by the direct dissolution method. The surfactant properties of the amphiphilic copolymers in PBS ( $10 \text{ mg mL}^{-1}$ ) were used to directly solubilize the solid curcumin ( $12 \text{ mg mL}^{-1}$ ) upon heating and vortexing, leading to drug loadings around 15 wt% (Figure 5A,B; Table S7, Supporting Information), which is similar as observed for the rehydration method with low DP polymers. Interestingly, there was no significant difference in drug loadings between gradient, respectively block copolymer-based systems, nor for the copolymers with different DP above DP 60; only the very short polymers (DP 40) showed lower drug loading, presumably due to the lower stability of the DP 40 micelles. It can be assumed that the DL values obtained by direct dissolution depend on the ratio of hydrophobic/hydrophilic segments rather than the copolymer architecture. This was supported by a drug loading experiment using a gradient copolymer with a higher content of hydrophobic PPhOx (G<sub>60</sub>5), which led to higher curcumin loading (18.1 wt% compared to 15.0 wt% for G5). The size of the curcumin-loaded nanoparticles was slightly larger compared to drug-free micelles, as determined by DLS measurements (Figure 5E,F; Figure S7 and Table S9, Supporting Information). Their morphology follows a similar pattern as observed for the unloaded micelles. All gradient copolymer-based formulations formed spherical micelles, while the block copolymer micelles formed a mixture of spherical and worm-like micelles in which the fraction of worm-like micelles increases with increasing copolymer DP.

Next, the stability of the G5 and B5-based curcumin nanoformulations was studied in solution (Figure 5C). A minor, insignificant, drop in curcumin content was observed after incubation of as-prepared nanoformulations at room temperature for 30 d, indicating excellent stability of the system, with no significant difference between gradient and block copolymer-based systems. For storage and transport purposes, the curcumin nanoformulations can be freeze-dried. The redissolution of the solid formulations obtained by the direct freeze-drying of G5, respectively B5-based nanoformulations led to the solutions containing nearly the same amount of solubilized curcumin as the samples before freeze-drying (Figure 5D). In summary, direct drug loading proved as a superior method for loading curcumin into PMeOx–PPhOx copolymer nanoparticles. The only drawback consists in relatively longer encapsulation times (72 h) needed for saturation of micelles with curcumin. This can be partly eliminated by predissolving

the curcumin in a meager amount of dimethyl sulfoxide (DMSO). After adding the micelles solution in PBS, the curcumin forms a fine suspension that is quickly uptaken by nanoparticles, reducing the encapsulation time to less than 30 min. The drug loadings obtained by this method were similar to the values obtained by the DMSO-free method (Figure S6, Supporting Information). The relative content of DMSO in nanoformulations is low (<3% v/v). Finally, a popular nanoprecipitation method was used to prepare curcumin-loaded nanoformulations, resulting in slightly higher drug loadings ( $\approx 16$  wt%, Table S8, Supporting Information). Herein, a mixture of the copolymer with curcumin was nanoprecipitated from ethanol into PBS, followed by ethanol evaporation under vacuum. However, extreme care has to be taken during the evaporation process to avoid the formation of the dry, thin-film, which leads to a sparingly soluble precipitate as described above.

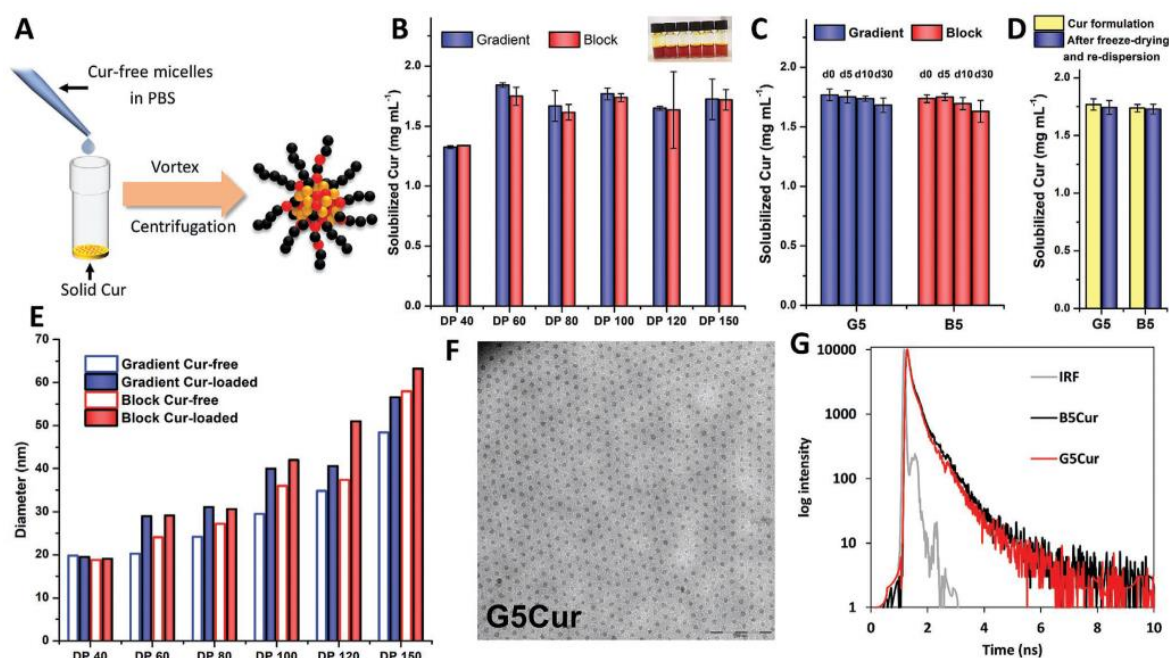


**Figure 5.** Solubilization of curcumin by PMeOx-PPhOx ( $F_{MeOx} = 0.7$ ) gradient (G2-G7) or diblock (B2-B7) copolymers using the direct dissolution method. (A) Schematic illustration of the loading of curcumin in preformed micelles. (B) The maximal amount of curcumin solubilized by amphiphilic copolymers ( $c_{pol} = 10$  mg mL<sup>-1</sup>) in PBS using an excess feed of curcumin (12 mg mL<sup>-1</sup>). (C) Stability of G5, respectively B5 curcumin nanoformulations in PBS 5, 10 and 30 days after loading. (D) Amount of curcumin solubilized by G5, respectively B5, before and after freeze-drying and re-dispersion ( $c_{pol} = 10$  mg mL<sup>-1</sup>). (E) The hydrodynamic diameter of the G2-G7, respectively B2-B7 nanoparticles before and after curcumin loading ( $c_{pol} = 10$  mg mL<sup>-1</sup>). (F) Cryo-TEM image of curcumin-loaded G5 nanoparticles (scale bar 200

nm). (G) Fluorescence decay curves for curcumin-loaded G5 and B5 with  $\lambda_{\text{ex}} = 405$  nm, the decays were monitored at 620 nm.

To conclude, the direct dissolution of curcumin by an aqueous gradient or block copolymer solution provides straightforward access to nanoformulations with decent loading of a hydrophobic drug. For instant clinical application, predissolving curcumin in a small amount of DMSO leads to the nanoformulations in a short time (<30 min). When storage of the solid freeze-dried nanoparticles is needed, the direct dissolution of solid curcumin by the copolymer micelles is preferred, however, at the cost of a longer encapsulation time. These DMSO-free samples were then used for further investigations, from now on abbreviated as, e.g., B5Cur, G5Cur, and G<sub>60</sub>5Cur representing nanoformulations based on copolymer B5, G5 respectively G<sub>60</sub>5. Interestingly, we have shown that the copolymer architecture does not play a significant role in the maximal curcumin loading, as both gradient and diblock analogs show similar drug loadings. These results are in line with the recently published study by Hrubý et al.[40] On the other hand, the drug loading can be improved by increasing the amount of PPhOx in the copolymer. This suggests that the curcumin loading depends on the hydrophobic/hydrophilic ratio of the amphiphilic copolymers rather than the monomer distribution or chain length.

## 2.5. Spectroscopic characteristics of nanoformulations

Six formulations were selected for the spectroscopic studies of the curcumin-loaded micelles, namely B2Cur, G2Cur, and G<sub>60</sub>2Cur (DP 40) as well as B5Cur, G5Cur, and G<sub>60</sub>5Cur (DP 100). Two examples of the absorption spectra for the micelles in PBS are shown in Figure S8A in the Supporting Information. In aqueous buffers, the absorption spectra of free curcumin exhibit a characteristic broad peak at 430 nm and a small shoulder at 355 nm. In the PMeOx–PPhOx micelles, the broad peak around 430 nm becomes prominent, and the shoulder peak at 355 nm disappears with the appearance of a new shoulder at 450 nm. These changes in the absorption spectrum indicate that curcumin is in a nonpolar-like environment. Minor differences in the maximum absorption wavelength were observed for the present samples (Table S10, Supporting Information). For DP = 40, the absorption maximum is always at 2–4 nm shorter wavelength as for the corresponding DP = 100 system, whereas for the MeOx molar content of 0.7, the absorption maximum is at  $\approx 5$  nm shorter wavelength than for 0.6. The absorption spectra for the corresponding block polymer and gradient polymer were equal, implying that curcumin is not entirely buried inside the PPhOx core but interacts with water.

In a nonpolar environment, the fluorescence spectrum of curcumin blue-shifts to 500 nm compared to 550 nm in an aqueous solution. However, the fluorescence spectra of the curcumin-loaded micelles (Figure S8B, Supporting Information) exhibit a considerable red shift having their maxima close to 620 nm. This can be explained by the well-known keto–enol tautomerism of curcumin, which induces aggregation and causes a significant decrease in the fluorescence intensity accompanied by a red-shifted fluorescence. The micelles with DP = 100 have higher relative fluorescence efficiency,  $\phi_{\text{rel}}$ , and their fluorescence maximum is at shorter wavelengths than those with DP = 40. This could indicate that curcumin is more aggregated in the micelles resulting from shorter copolymers with DP 40 and/or in a more polar environment. For the systems based on copolymers with a MeOx molar content of 0.7, the  $\phi_{\text{rel}}$  is lower than for corresponding micelles with a MeOx molar content of 0.6. Also, the block copolymer micelles have higher relative fluorescence efficiency than the corresponding gradient polymer.

The fluorescence decays of curcumin measured for the selected formulations show a multiexponential behavior (Figure S8C, Supporting Information). This is typical for curcumin systems since its fluorescence lifetime varies with changes in, for example, viscosity, polarity, and hydrogen-bonding ability of the environment. In the present study, the lifetime values were obtained by fitting the decays with the three-exponential decay model (Equation S1, Supporting Information) (and are tabulated in Table S10 in the Supporting Information). The shortest  $\approx 100$  ps component dominates the decays with  $\approx 10$ – $20\%$  contribution of the  $\approx 450$  ps component. The proportion of the longest-living 0.8–1.5 ns component is very small ( $\approx 0.1\%$ ), but without its presence, it was not possible to obtain acceptable fitting results. This minor population could represent small amounts of monomeric curcumin molecules in a highly nonpolar environment. The observed complex fluorescence decay curves suggest a local heterogeneity in the distribution and degree of aggregation of the curcumin inside the micelles. When comparing the different formulations, it is simpler to consider the average fluorescence lifetimes  $\langle \tau \rangle$  (Table S10, Supporting Information) instead of emphasizing all the decay components. The  $\langle \tau \rangle$  is shorter for systems based on copolymers with a MeOx molar content of 0.7 than for corresponding micelles with a MeOx molar content of 0.6. Also,  $\langle \tau \rangle$  are  $\approx 50$  ps longer for micelles based on copolymers with a DP of 100 compared to polymers with a DP of 40. As a summary, the spectroscopic studies of the curcumin-loaded micelles indicate that in micelles based on copolymers with a DP of 100 the curcumin is more shielded from the polar environment than in the micelles based on copolymers with a DP of 40. Also, according to the

fluorescence measurements, there is a small difference between the block polymer and gradient copolymer micelles: either the curcumin is less aggregated or better shielded in the block copolymer micelles.

## **2.6. In vitro drug release**

The release of curcumin from the nanoformulations was studied in PBS at 37 °C using a dialysis method. A relatively high molecular weight cut-off dialysis membrane (50 kDa) was selected to mimic the sink conditions in vivo and ensure the rapid permeability of both released curcumin and macromolecular unimers. Generally, two main mechanisms contribute to the drug release from the micellar formulation. In the beginning, the diffusion-driven leaching of the drug from the outer parts of the core results in so-called “burst release,” which leads to the rapid loss of a significant part of the drug cargo. This is considered one of the main drawbacks of micellar nanoformulation systems.[48] After this initial release, the remaining drug is trapped inside the hydrophobic core and the diffusion-driven release is slowed down. At this moment, the micelle disassembly, due to the micelle-unimer equilibrium, mostly drives the drug release. From the biomedical point of view, the ideal micellar system should combine low burst drug release with sustained release afterward. Comparing the curcumin release from the synthesized gradient and block copolymer nanoformulations G2Cur, B2Cur, G5Cur, and B5Cur revealed a relatively small burst release ( $\approx 12\%$  of curcumin released after 2 h of incubation), which is statistically independent of the copolymer architecture and length. This can be explained by several factors, such as the rigidity of the micellar core, interactions between curcumin and the aromatic core, as well as the relatively low drug loading. On the other hand, upon longer incubation times, faster drug release was observed from the gradient copolymer formulations, presumably due to their lower stability. This corroborates the fact that the less stable shorter-DP micelles release curcumin faster than their longer polymer analogs. The faster sustained drug release from the gradient copolymer nanoformulations might be beneficial for the pharmacokinetic profile of the carried drug.

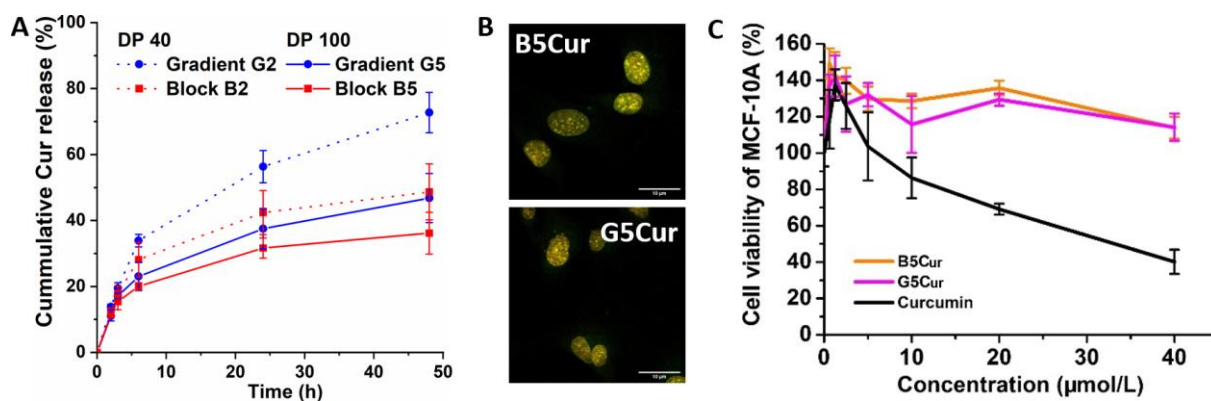


**Figure 6.** A) Release of curcumin from micellar nanoformulations in PBS (pH = 7.4, 37 °C). B) Uptake of curcumin nanoformulations B5Cur, respectively G5Cur into MDA-MB-231 cells after 2 h of incubation. Scale bars represent 10 µm. C) Viability of MCF-10A cells after 48 h incubation with nanoformulations loaded by B5Cur or G5Cur and free curcumin, respectively. The concentrations refer to curcumin content. All data are expressed as mean ± SD (n = 3–6).

## 2.7. In vitro biological evaluation

For application as drug delivery vehicles, the nanoformulations should be rapidly internalized by cells. This was confirmed by confocal microscopy, which confirmed the rapid internalization of the curcumin-loaded nanoformulations G5Cur and B5Cur by MDA-MB-231 cells upon short incubation times (2 h, Figure 6B). Furthermore, the cytotoxicity of G5Cur, B5Cur, and free curcumin was evaluated by an in vitro experiment using normal breast MCF-10A cells and breast cancer MDA-MB-231 cells, respectively (Figure 6C; Figure S9, Supporting Information). The cells were incubated in the presence of the copolymer nanoformulations for 48 h at 37 °C, after which the cell viability was assessed by WST-1 assay. The results showed that in MCF-10A cells, curcumin-loaded B5Cur and curcumin-loaded G5Cur have no cytotoxicity, while the free curcumin has significant cytotoxicity with increasing concentration ( $P < 0.0001$ ). On the other hand, MDA-MB-231 cells are less sensitive to free curcumin. Within the studied concentration range, free curcumin, as well as curcumin-loaded B5Cur and G5Cur, show very similar cytotoxicity profiles, with signs of cytotoxicity observed only for the highest concentrations tested. These results suggest that there are no significant differences between both curcumin-loaded B5Cur and G5Cur and underline the potential of amphiphilic gradient copolymers as drug delivery vehicles.

### **3. Conclusions**

In summary, we studied aqueous self-assembly and hydrophobic drug encapsulation of a series of amphiphilic gradient copoly(2-oxazoline)s with different chain lengths and compared them to diblock copolymer analogs. We observed strong dependence of the self-assembly characteristics on the total polymer length. While shorter block and gradient copolymers with a DP below 60 self-assembled into micelles of nearly the same size, the micelles formed by the longer copolymers were found to be smaller for the gradient copolymers compared to the block copolymers. The stability of the nanoparticles showed chain length dependence, with gradient copolymer micelles being more dynamic and slightly less stable than block analogs but still sufficiently stable for intended biomedical applications. The potential of the prepared copolymers as drug delivery systems was thoroughly examined using model drug curcumin. Three different methods for drug-loaded nanoformulations fabrication were studied, where the direct encapsulation of solid curcumin by preassembled micelles provided the best results. The prepared nanoformulations were stable upon storage, showed significant cellular uptake and cytotoxicity. Interestingly, there were no significant differences between the maximal drug loadings of analogous gradient and diblock copolymer nanoparticles. Considering their straightforward single-step synthesis, gradient copolymer nanoformulations represent an attractive alternative to block copolymer amphiphiles for the construction of novel drug delivery systems. To fully evaluate their biomedical potential, further biological assessment of gradient copolymer nanoparticles will be necessary in future work, including in vivo toxicity, immunogenicity, pharmacokinetics, and therapeutic effectivity.

### **Acknowledgements**

R.H. thanks FWO and Ghent University for continuous financial support. O.S. acknowledges the funding from the FWO and Charles University Prague (grant PRIMUS/21/SCI/007). S.F. acknowledges the Leverhulme Trust for the visiting professorship grant (VP2-2020-013) to support the visit and work of S.F. at the University of Reading.

### **References**

- [1] S. Tonge, B. Tighe, *Adv. Drug Delivery Rev.* 2001, 53, 109.
- [2] S. Garnier, A. Laschewsky, *Langmuir* 2006, 22, 4044.
- [3] K. Letchford, H. Burt, *Eur. J. Pharm. Biopharm.* 2007, 65, 259.
- [4] I. F. Uchegbu, S. P. Vyas, *Int. J. Pharm.* 1998, 172, 33.

- [5] Y. Mai, A. Eisenberg, *Chem. Soc. Rev.* 2012, 41, 5969.
- [6] A. Blanz, S. P. Armes, A. J. Ryan, *Macromol. Rapid Commun.* 2009, 30, 267.
- [7] K. Nakashima, P. Bahadur, *Adv. Colloid Interface Sci.* 2006, 123, 75.
- [8] K. Kataoka, A. Harada, Y. Nagasaki, *Adv. Drug Delivery Rev.* 2012, 64, 37.
- [9] J. I. Hare, T. Lammers, M. B. Ashford, S. Puri, G. Storm, S. T. Barry, *Adv. Drug Delivery Rev.* 2017, 108, 25. [10] Y. Chen, H. Chen, M. Feng, Y. Dong, *Eur. Polym. J.* 2016, 85, 489.
- [10] Y. Chen, H. Chen, M. Feng, Y. Dong, *Eur. Polym. J.* 2016, 85, 489.
- [11] M. M. Alam, K. S. Jack, D. J. Hill, A. K. Whittaker, H. Peng, *Eur. Polym. J.* 2019, 116, 394.
- [12] Z. Deng, Q. Shi, J. Tan, J. Hu, S. Liu, *ACS Mater. Lett.* 2021, 3, 1339.
- [13] J. Zhang, B. Farias-Mancilla, M. Destarac, U. S. Schubert, D. J. Keddie, C. Guerrero-Sanchez, S. Harrisson, *Macromol. Rapid Commun.* 2018, 39, 1800357.
- [14] R. Yañez-Macias, I. Kulai, J. Ulbrich, T. Yildirim, P. Sungur, S. Hoepfener, R. Guerrero-Santos, U. S. Schubert, M. Destarac, C. Guerrero-Sanchez, *Polym. Chem.* 2017, 8, 5023.
- [15] S. Agarwal, *Polym. Chem.* 2010, 1, 953.
- [16] T. Gleede, E. Rieger, J. Blankenburg, K. Klein, F. R. Wurm, *J. Am. Chem. Soc.* 2018, 140, 13407.
- [17] T. Gleede, J. C. Markwart, N. Huber, E. Rieger, F. R. Wurm, *Macromolecules* 2019, 52, 9703.
- [18] E. Galanos, E. Grune, C. Wahlen, A. H. Müller, M. Appold, M. Gallei, H. Frey, G. Floudas, *Macromolecules* 2019, 52, 1577.
- [19] S. K. Filippov, B. Verbraeken, P. V. Konarev, D. I. Svergun, B. Angelov, N. S. Vishnevetskaya, C. M. Papadakis, S. Rogers, A. Radulescu, T. Courtin, J. C. Martins, L. Starovoytova, M. Hruby, P. Stepanek, V. S. Kravchenko, I. I. Potemkin, R. Hoogenboom, J. *Phys. Chem. Lett.* 2017, 8, 3800.
- [20] H. M. Lambert-Thijs, M. J. Jochems, R. Hoogenboom, U. S. Schubert, *J. Polym. Sci., Part A: Polym. Chem.* 2009, 47, 6433.

- [21] R. Hoogenboom, M. W. Fijten, S. Wijnans, A. M. van den Berg, H. M. Thijs, U. S. Schubert, *J. Comb. Chem.* 2006, 8, 145.
- [22] O. Sedlacek, K. Lava, B. Verbraeken, S. Kasmi, B. G. De Geest, R. Hoogenboom, *J. Am. Chem. Soc.* 2019, 141, 9617.
- [23] P. H. Van Steenberge, B. Verbraeken, M.-F. o. Reyniers, R. Hoogenboom, D. R. D'hooge, *Macromolecules* 2015, 48, 7765.
- [24] D. Bera, O. Sedlacek, E. Jager, E. Pavlova, M. Vergaelen, R. Hoogenboom, *Polym. Chem.* 2019, 10, 5116.
- [25] R. Hoogenboom, *Angew. Chem., Int. Ed.* 2009, 48, 7978.
- [26] H. Schlaad, C. Diehl, A. Gress, M. Meyer, A. L. Demirel, Y. Nur, A. Bertin, *Macromol. Rapid Commun.* 2010, 31, 511.
- [27] T. Lorson, M. M. Lübtow, E. Wegener, M. S. Haider, S. Borova, D. Nahm, R. Jordan, M. Sokolski-Papkov, A. V. Kabanov, R. Luxenhofer, *Biomaterials* 2018, 178, 204.
- [28] B. Verbraeken, B. Monnery, K. Lava, R. Hoogenboom, *Eur. Polym. J.* 2017, 88, 451.
- [29] M. Glassner, M. Vergaelen, R. Hoogenboom, *Polym. Int.* 2018, 67, 32.
- [30] G. Morgese, B. Verbraeken, S. N. Ramakrishna, Y. Gombert, E. Cavalli, J. G. Rosenboom, M. Zenobi-Wong, N. D. Spencer, R. Hoogenboom, E. M. Benetti, *Angew. Chem., Int. Ed.* 2018, 57, 11667.
- [31] O. Sedlacek, R. Hoogenboom, *Adv. Ther.* 2020, 3, 1900168.
- [32] O. Sedlacek, A. Van Driessche, A. Uvyn, B. G. De Geest, R. Hoogenboom, *J. Controlled Release* 2020, 326, 53.
- [33] R. Luxenhofer, A. Schulz, C. Roques, S. Li, T. K. Bronich, E. V. Batrakova, R. Jordan, A. V. Kabanov, *Biomaterials* 2010, 31, 4972.
- [34] Z. He, A. Schulz, X. Wan, J. Seitz, H. Bludau, D. Y. Alakhova, D. B. Darr, C. M. Perou, R. Jordan, I. Ojima, *J. Controlled Release* 2015, 208, 67.
- [35] M. M. Lübtow, L. Hahn, M. S. Haider, R. Luxenhofer, *J. Am. Chem. Soc.* 2017, 139, 10980.

- [36] Z. He, X. Wan, A. Schulz, H. Bludau, M. A. Dobrovolskaia, S. T. Stern, S. A. Montgomery, H. Yuan, Z. Li, D. Alakhova, M. Sokolsky, D. B. Darr, C. M. Perou, R. Jordan, R. Luxenhofer, A. V. Kabanov, *Biomaterials* 2016, 101, 296.
- [37] X. Wan, J. J. Beaudoin, N. Vinod, Y. Min, N. Makita, H. Bludau, R. Jordan, A. Wang, M. Sokolsky, A. V. Kabanov, *Biomaterials* 2019, 192, 1.
- [38] V. S. Kravchenko, I. I. Potemkin, *J. Phys. Chem. B* 2016, 120, 12211.
- [39] S. Datta, A. Jutková, P. Šrámková, L. Lenkavská, V. Huntošová, D. Chorvát, P. Miškovský, D. Jancura, J. Kronek, *Biomacromolecules* 2018, 19, 2459.
- [40] L. Loukotová, P. Švec, O. Groborz, T. Heizer, H. Beneš, H. Raabová, T. Bělinová, V. Herynek, M. Hrubý, *Macromolecules* 2021, 54, 8182.
- [41] R. Lund, L. Willner, J. Stellbrink, A. Radulescu, D. Richter, *Macromolecules* 2004, 37, 9984.
- [42] H. Cabral, K. Miyata, K. Osada, K. Kataoka, *Chem. Rev.* 2018, 118, 6844.
- [43] L. G. Chen, H. Bermudez, *Langmuir* 2012, 28, 1157.
- [44] K. Florey, *Analytical Profiles of Drug Substances, Vol. 5*. Elsevier Science & Technology, Amsterdam, Netherlands 1976.
- [45] K. Suresh, A. Nangia, *CrystEngComm* 2018, 20, 3277.
- [46] Z. He, X. Wan, A. Schulz, H. Bludau, M. A. Dobrovolskaia, S. T. Stern, S. A. Montgomery, H. Yuan, Z. Li, D. Alakhova, *Biomaterials* 2016, 101, 296.
- [47] M. M. Lübtow, M. S. Haider, M. Kirsch, S. Klisch, R. Luxenhofer, *Biomacromolecules* 2019, 20, 3041.
- [48] J. Liu, H. Lee, C. Allen, *Curr. Pharm. Des.* 2006, 12, 4685.